published by Ural Federal University
eISSN 2411-1414
chimicatechnoacta.ru

ARTICLE
2024, vol. 11(4), No. 202411418
DOI: 10.15826/chimtech.2024.11.4.18

Synthesis and selective Cu(II) complexation of lower rim substituted thiacalixarenes containing pyrazole fragments

Valeriy Kalinin [a], Ekaterina Rasperetikhina [a], Mikhail Bukharov [a], Ksenia Shibaeva [a], Daut Islamov [b], Olga Babaeva [c], Ivan Stoikov [a] *

a: A. M. Butlerov Chemical Institute, Kazan Federal University, 420008 Kazan, Russia
b: Laboratory for structural analysis of biomacromolecules, FRC Kazan Scientific Center, Russian Academy of Sciences, 420008 Kazan, Russia
c: A. E. Arbuzov Institute of Organic and Physical Chemistry, FRC Kazan Scientific Center, Russian Academy of Sciences, 420088 Kazan, Russia
* Corresponding author: ivan.stoikov@mail.ru

This paper belongs to a Regular Issue.

Abstract

Selective sensors for the detection and quantification of Cu(II) ions are actively used to investigate in vivo conditions in Wilsons and Menkes diseases at the cellular level. Such sensors must have a high specificity for this cation as well as low toxicity. A synthetic approach for the preparation of selective sensors for Cu(II) cations based on *p-tert*-butylthiacalix[4]arenes modified with 3,5-dimethylpyrazole moieties in *cone*, *partial cone* and *1,3-alternate* stereoisomeric forms was developed. The obtained compounds were characterized by single-crystal XRD, NMR and IR spectroscopy, MALDI MS, and elemental analysis. All synthesized thiacalixarene compounds formed complexes with Cu(II) with the binding constants in range log$K$ = 4.44–4.63 and 1:1 stoichiometry. The structure of the obtained complexes was studied by NMR spectroscopy and DFT methods. The obtained results can be used to develop selective Cu(II) sensors.

Keywords

thiacalixarenes
pyrazoles
synthesis
Cu(II) cation
sensors
selectivity

Received: 14.11.24
Revised: 21.11.24
Accepted: 21.11.24
Available online: 27.11.24

Key findings

- New 3,5-dimethylpyrazole derivatives of *p-tert*-butylthiacalix[4]arenes were obtained and characterized by instrumental methods.
- Selective binding of all obtained derivatives of thiacalix[4]arenes to Cu(II) cations was shown by UV-Vis and NMR methods. The binding constants were calculated.
- The structures of the Cu(II) complex were modeled for the monomeric compound by the DFT method.

Supplementary materials

1. Introduction

Copper-related diseases are pathological disorders that result from an impaired metabolism of copper compounds. Such diseases include genetic disorders associated with impaired copper metabolism, e.g., Wilson's and Menkes diseases [1, 2]. Wilson's disease is characterized by an excess of copper in tissues, which culminates in liver cirrhosis due to an elevated concentration of redox-active copper cations. In Wilson's disease, the defective ATP7B protein is unable to excrete excess copper into the bile, resulting in its toxic accumulation. Excess copper creates reactive oxygen species, leading to oxidative stress and damage to cellular structures including lipids, proteins and DNA. These cations have the capacity to destroy hepatic proteins [3]. In contrast, Menkes disease is characterized by a significant reduction in the concentration of copper cations in certain tissues. In Menkes disease, there is dysfunction of the ATP7A protein, which interferes with the normal absorption of copper from the intestine and its distribution to various tissues. As a result, copper levels in many organs become critically low [4]. Both diseases can be identified at the earliest stages, and the treatment is primarily symptomatic, aiming to correct copper concentrations in biological media [5]. Furthermore, there is evidence to suggest that a number of neuro-

degenerative diseases, including Alzheimer's disease [6], Parkinson's disease [7], and Creutzfeldt-Jakob disease [8], are also associated with pathological interactions of proteins with copper cations. Furthermore, there is evidence that copper complex compounds have pharmacological effects, particularly anti-cancer, anti-diabetic and disinfectant activity [9]. The control of copper concentration in biological tissues has been identified as the most crucial stage of copper-related diseases diagnostics, enabling the determination of copper concentrations at an early stage and the commencement of treatment [10]. To achieve these objectives, a sensor with high selectivity to copper cations, low detection limit, and low toxicity should be used.

It is well established that pyrazole derivatives are among the most effective ligands due to their simple preparation methods, complexation capabilities, and favorable biological properties [11]. Pyrazole derivatives are particularly prevalent as ligands for a range of metal cations [12], anions [13], and organic molecules [14]. Furthermore, pyrazole derivatives were demonstrated to possess antipyretic [15], antimalarial [16], anticancer [17], analgesic [18], and antiviral [19] properties. Pyrazole derivatives include a variety of compounds including phenazone, aminophenazone, methamisole and others [20–22].

Calixarene and its sulfur-containing analogue, thiacalixarene, are examples of supramolecular platforms that have a broad range of applications due to their low toxicity, the potential for partial or complete substitution, and the ability to be organized in various stereoisomeric forms (*cone*, *1,3-alternate*, and, to a lesser extent, *partial cone* and *1,2-alternate*) [23, 24]. In comparison with its classical methylene analogue, *p-tert*-butylthiacalix[4]arene exhibits a larger cavity size, the presence of additional binding centres in the form of four sulfur atoms and greater availability of configurations [25]. *p-tert*-Butylthiacalix[4]arene serves as the foundation for numerous biologically active compounds, including those with anticancer properties [26], bactericidal capabilities [27, 28], the ability to inhibit lysozyme fibrillation [29], etc. Pyrazole derivatives of calixarenes have been previously reported [30], but the authors did not go further than the synthesis, limiting themselves to a short communication. The complexation properties of the obtained compounds were also not investigated. In recent years, new data on pyrazole-containing (thia)calixarenes has appeared. Thus, in the work [31], the pyrazole cycle was obtained due to the interaction of triple alkynyl linkage with hydrazine hydrate. In [32], the already prepared pyrazole fragment was introduced by Williamson synthesis. However, in general, it can be concluded that pyrazole is a rather rare substituent fragment in these macrocycles.

The combination of 3,5-dimethylpyrazole with the macrocyclic platform of *p-tert*-butylthiacalix[4]arene represents a promising integration of the advantages inherent to both structural motifs. The thiacalixarene platform endows the resulting compound with the properties of a host molecule, including the presence of convergent binding centers capable of forming supramolecular ensembles. Additionally, the 3,5-dimethylpyrazole residue confers sensory properties to the hybrid structure. The study of metal complexation properties of (thia)calixarenes is very attractive to many research groups [33–62]. The findings of the study may open up opportunities for the development of new Cu(II) sensors and bioactive copper-containing heterocyclic compositions.

2. Materials and Methods

2.1. General

Detailed information about the used reagents and equipment, research methodology and data processing can be found in the Supplementary Information. References [63–75] are also mentioned in the Supplementary Information.

2-(4-(*tert*-Butyl)phenoxy)acetohydrazide (**Hyd-mono**) was obtained by analogy with the literature procedure [76]. **Hyd-cone**, **Hyd-paco**, and **Hyd-alt** were synthesized earlier in our research group [44].

2.2. Synthesis of 2-(4-(*tert*-butyl)phenoxy)-1-(3,5-dimethyl-1H-pyrazol-1-yl)ethan-1-one (Pyr-mono)

To a solution of 2-(4-(*tert*-butyl)phenoxy)acetohydrazide (**Hyd-mono**) (1.00 g, 4.50 mmol) in chloroform (10 mL) and acetylacetone (1.8 mL, 18 mmol), *p*-toluenesulfonic acid (5 mol%) was added. The reaction mixture was refluxed for 24 hours. The resulting solution was evaporated to dryness to an oil, crystallized from isopropanol, filtered and washed with isopropanol.

White powder, yield: 0.83 g (70%), m_p 59 °C. ^{1}H NMR (400 MHz, 298K, $CDCl_3$): 1.29 (*s*, 9H, *t*-Bu), 2.26 (*s*, 3H, Pyr-CH_3), 2.57 (*s*, 3H, Pyr-CH_3), 5.41 (*s*, 2H, O–CH_2–), 6.00 (*s*, 1H, Pyr-H), 6.92 (*s*, 2H, Ar-H), 7.30 (*s*, 2H, Ar-H).

^{13}C{^{1}H} NMR (100 MHz, 298K, $CDCl_3$): 14.1., 35.5, 66.7, 111.2, 114.2, 126.3, 144.5, 153.2, 155.7, 168.4

FTIR ATR, cm^{-1}: 1590 (C=N), 1750 (C=O).

MALDI MS: Calculated: $[M + H]^+$ m/z = 287.2, $[M + Na]^+$ m/z = 309.2, $[M + K]^+$ m/z = 325.1. Found: $[M + H]^+$ m/z = 286.9, $[M + Na]^+$ m/z = 308.9, $[M + K]^+$ m/z = 324.9.

Elemental analysis: Calculated: C – 71.30%, H – 7.74%, O – 11.17%, N – 9.79%. Found: C – 71.34%, H – 7.69%, O – 11.21%, N – 9.76%.

2.3. Synthesis of 5,11,17,23-tetra-*tert*-butyl-25,26,27,28-tetrakis-[(3,5-dimethylpyrazol-1-ylcarbonyl)methoxy]thiacalix[4]arene in *cone* conformation (Pyr-cone)

To a solution of **Hyd-cone** (0.50 g, 0.40 mmol) in chloroform (1 mL) and acetylacetone (0.80 mL, 7.90 mmol), *p*-toluenesulfonic acid (5 mol%) was added. The reaction mixture was refluxed for 24 h. The resulting

 DOI: 10.15826/chimtech.2024.11.4.18

precipitate was filtered off, washed with methanol and recrystallized from methanol:chloroform mixture.

White powder, yield: 0.40 g (64%), m_p 250 °C.

^{1}H NMR (400 MHz, 298K, $CDCl_3$): 1.09 (*s*, 36H, *t*-Bu), 1.98 (*s*, 12H, Pyr-CH_3), 2.39 (*s*, 12H, Pyr-CH_3), 5.79 (*s*, 4H, Pyr-H), 6.32 (*s*, 8H, O–CH_2–), 7.31 (*s*, 8H, Ar–H).

^{13}C{^{1}H} NMR (100 MHz, 298K, $CDCl_3$): 13.8, 14.0, 31.2, 34.1, 72.0, 110.0, 129.3, 134.5, 143.7, 146.0, 151.7, 157.6, 169.2

FTIR ATR, cm^{-1}: 1590 (C=N), 1750 (C=O).

MALDI MS: Calculated: $[M + Na]^+$ *m*/*z* = 1287.5, $[M + K]^+$ *m*/*z* = 1303.5. Found: $[M + Na]^+$ *m*/*z* = 1287.4, $[M + K]^+$ *m*/*z* = 1303.4.

Elemental analysis: Calculated: C – 57.12%, H – 6.39%, O – 12.68%, N – 11.10%, S – 12.71%. Found: C – 57.19%, H – 6.41%, O – 12.54%, N – 11.12%, S – 12.74%.

2.4. Synthesis of 5,11,17,23-tetra-*tert*-butyl-25,26,27,28-tetrakis-[(3,5-dimethylpyrazol-1-ylcarbonyl)methoxy]thiacalix[4]arene in *partial cone* conformation (Pyr-paco)

To a solution of **Hyd-paco** (0.50 g, 0.40 mmol) in isopropanol (5 mL) and acetylacetone (0.80 mL, 7.90 mmol), *p*-toluenesulfonic acid (5 mol%) was added. The reaction mixture was refluxed for 12 h. The resulting precipitate was filtered off, washed with methanol and recrystallized from the methanol : chloroform mixture.

White powder, yield: 0.51 g (82%), m_p 216 °C.

^{1}H NMR (400 MHz, 298K, $CDCl_3$): 1.07 (*s*, 18H, *t*-Bu), 1.33 (*s*, 9H, *t*-Bu), 1.35 (*s*, 9H, *t*-Bu), 2.09 (*s*, 3H, Pyr-CH_3), 2.16 (*s*, 6H, Pyr-CH_3), 2.20 (*s*, 3H, Pyr-CH_3), 2.25 (*s*, 3H, Pyr-CH_3), 2.47 (*s*, 6H, Pyr-CH_3), 2.58 (*s*, 3H, Pyr-CH_3), 5.50 (*s*, 2H, O–CH_2), 5.52 (*d*, $^3J_{HH}$ = 16.9 Hz, 2H, O–CH_2), 5.69 (*d*, $^3J_{HH}$ = 16.9 Hz, 2H, O–CH_2), 5.79 (*s*, 1H, Pyr-H), 5.92 (*s*, 2H, Py-H), 5.96 (*s*, 2H, O–CH_2), 5.99 (*s*, 1H, Pyr-H), 7.11 (*d*, $^3J_{HH}$ = 2.4 Hz, 2H, Ar–H), 7.45 (*d*, $^3J_{HH}$ = 2.4 Hz, 2H, Ar–H), 7.62 (*s*, 2H, Ar-H), 7.88 (*s*, 2H, Ar-H).

^{13}C{^{1}H} NMR (100 MHz, 298K, $CDCl_3$): 13.8, 30.8, 34.2, 68.7, 69.9, 72.1, 110.5, 128.2, 129.0, 134.2, 135.2, 143.9, 146.5, 150.5, 152.0, 157.9, 166.9, 167.7, 170.3.

FTIR ATR, cm^{-1}: 1581 (C=N), 1750 (C=O).

MALDI MS: Calculated: $[M + Na]^+$ *m*/*z* = 1287.5. Found: $[M + Na]^+$ *m*/*z* = 1287.4.

Elemental analysis: Calculated: C – 57.12%, H – 6.39%, O – 12.68%, N – 11.10%, S – 12.71%. Found: C – 57.10%, H – 6.32%, O – 12.54%, N – 11.21%, S – 12.83%.

2.5. Synthesis of 5,11,17,23-tetra-*tert*-butyl-25,26,27,28-tetrakis-[(3,5-dimethylpyrazol-1-ylcarbonyl)methoxy]thiacalix-[4]arene in *1,3-alternate* conformation (Pyr-alt)

To a solution of **Hyd-alt** (0.50 g, 0.40 mmol) in isopropanol (5 mL) and acetylacetone (0.80 mL, 7.90 mmol), *p*-toluenesulfonic acid (5 mol%) was added. The reaction mixture was refluxed for 24 h. The resulting precipitate was filtered off, washed with methanol and recrystallized from the methanol: chloroform mixture.

White powder, yield: 0.54 g (87%), m_p 278 °C.

^{1}H NMR (400 MHz, 298K, $CDCl_3$): 1.26 (*s*, 36H, *t*-Bu), 2.19 (*s*, 12H, Pyr-CH_3), 2.63 (*s*, 12H, Pyr-CH_3), 5.45 (*s*, 8H, O–CH_3), 5.98 (*s*, 4H, Pyr-H), 7.74 (*s*, 8H, Ar-H).

^{13}C{^{1}H} NMR (100 MHz, 298K, $CDCl_3$): 14.0, 14.5, 31.5, 34.5, 69.7, 110.8, 128.3, 134.4, 144.4, 146.5, 152.1, 157.8, 167.2.

FTIR ATR, cm^{-1}: 1590 (C=N), 1753 (C=O).

MALDI MS: Calculated: $[M + H]^+$ *m*/*z* = 1265.5, $[M + Na]^+$ *m*/*z* = 1287.5, $[M + K]^+$ *m*/*z* = 1303.5. Found: $[M + H]^+$ m/z = 1265.6, $[M + Na]^+$ *m*/*z* = 1287.6, $[M + K]^+$ *m*/*z* = 1303.6.

Elemental analysis: Calculated: C – 57.12%, H – 6.39%, O – 12.68%, N – 11.10%, S – 12.71%. Found: C – 57.16%, H – 6.41%, O – 12.63%, N – 11.11%, S – 12.69%.

3. Results and Discussion

3.1. Synthesis of 3,5-dimethylpyrazole-modificated thiacalix[4]arenes

It was established that macrocyclic structures, including derivatives of (thia)calixarenes, are frequently employed to develop selective sensors for a range of substrates [38–40]. Pyrazole fragments are frequently incorporated into ligands capable of forming complexes with metal cations [41–43]. Thus it was reasonable to hypothesize that the introduction of a pyrazole heterocyclic fragment into the structure of *p-tert*-butylthiacalix[4]arene would result in the generation of ligands with high selectivity of binding to various substrates. It was suggested that the interaction with "soft" cations of transition metals such as Cu(II), Ni(II) and Ag(I) would be favorable due to the presence of a "soft" sulfur atom and pyrazole cycle in the structure of thiacalixarene, which is capable of coordination with the aforementioned cations.

The starting materials employed were hydrazides of thiacalixarenes in three stereoisomeric forms, i.e., *cone* (**Hyd-cone**), *partial cone* (**Hyd-paco**), and *1,3-alternate* (**Hyd-alt**) [44]. In that work, it was proposed that hydrazides of *p-tert*-butylthiacalix[4]arene have significant synthetic potential for the synthesis of new macrocyclic derivatives, given that the hydrazide fragment is amenable to various modifications, including alkylation [45], acylation [46] and cyclisation [47]. Hydrazides are convenient precursors for the preparation of 3,5-dimethylpyrazole derivatives, since the direct reaction with acetylacetone is carried out in high yields (Scheme 1). As a synthetic methodology, we initially relied on an article in which pyrazolides were prepared using the classical calixarene [30]. However, the protocol outlined in the article [30] proved unsuitable for the preparation of thiacalixarene derivatives, as inseparable mixtures of products were obtained. We found that the reaction in the case of the sulfur analogue of the macrocycle did not

 DOI: 10.15826/chimtech.2024.11.4.18

proceed in the absence of a catalyst. Consequently, an alternative approach was developed. Glacial acetic acid, trifluoroacetic acid and *p*-toluenesulfonic acid (PTSA) were tested as potential catalysts. PTSA was identified as the optimal catalyst for the synthesis of 3,5-dimethylpyrazole derivatives of thiacalixarene for all three conformations (**Pyr-cone**, **Pyr-paco**, and **Pyr-alt**). Initially, ethanol was applied as the reaction medium, but in all instances this approach proved ineffective failing to yield the desired final products. For example, **Pyr-paco** and **Pyr-alt** did not dissolve in ethanol when refluxed; therefore, a less polar solvent was used as an alternative. The solvents were selected so that the starting compounds dissolved and the products precipitated. The **Pyr-cone** took the shortest time to form precipitate, while the *1,3-alternate* took the longest time. The replacement of ethanol with isopropanol as a solvent to obtain hydrazides in *partial cone* and *1,3-alternate* conformations yielded favorable outcomes.

Use of any alcohols in case of **Pyr-cone** synthesis resulted in the formation of a complex mixture of products, which included alkoxy fragments. This indicates that the substitution reaction of the 3,5-dimethylpyrazole fragment with an alcohol molecule occurred. It was established that *cone* stereoisomeric form exhibits a higher reactivity than *partial cone* and *1,3-alternate*. Furthermore, 3,5-dimethylpyrazole is a suitable leaving group, which is employed on occasion to produce esters and amides [48]. Accordingly, the alcohols were replaced with chloroform, resulting in the production of **Pyr-cone** in a moderate yield. Upon prolonging the reaction time, the yield remained relatively constant, likely due to partial dissolution of the product. In general, thiacalixarenes in *cone* conformation with short substituents of approximately five carbon atoms in chain are more reactive than those in *partial cone* and *1,3-alternate* conformations. This can be explained by steric reasons. In *partial cone* and *1,3-alternate* conformations, a shielding effect involving *tert*-butyl groups is observed. The monomer compound **Pyr-mono** was obtained through a method analogous to that employed for **Pyr-cone**. The target compounds were synthesized in yields ranging from 64 to 87%. Their structures were confirmed by physical methods of investigation, including ^{1}H and ^{13}C{^{1}H} NMR, IR spectroscopy, mass spectrometry (MALDI MS), and elemental analysis (Figures S1–S16).

NMR spectroscopy represents an optimal methodology for elucidating the structural characteristics of the synthesized macrocyclic derivatives. As an illustration, the ^{1}H NMR spectrum of **Pyr-alt** exhibited signals attributed to the protons of *tert*-butyl groups (1.26 ppm), methyl groups in the pyrazole substituent (2.19 ppm and 2.63 ppm), oxymethylene groups (5.45 ppm), protons of the pyrazole fragment (5.98 ppm) and aromatic protons (7.74 ppm) (Figure S4).

NMR spectroscopy is capable of distinguishing the isomeric compounds that are in different conformations. Therefore, the signals for the *tert*-butyl fragments in **Pyr-cone** were observed at 1.09 ppm, while the methyl substituents in the 3,5-dimethylpyrazole fragment were recorded at 1.98 and 2.39 ppm. Additionally, the protons of the oxymethylene, pyrazole, and aryl fragments appear at 6.32 ppm, 5.79 ppm, and 7.31 ppm, respectively (Figure S2).

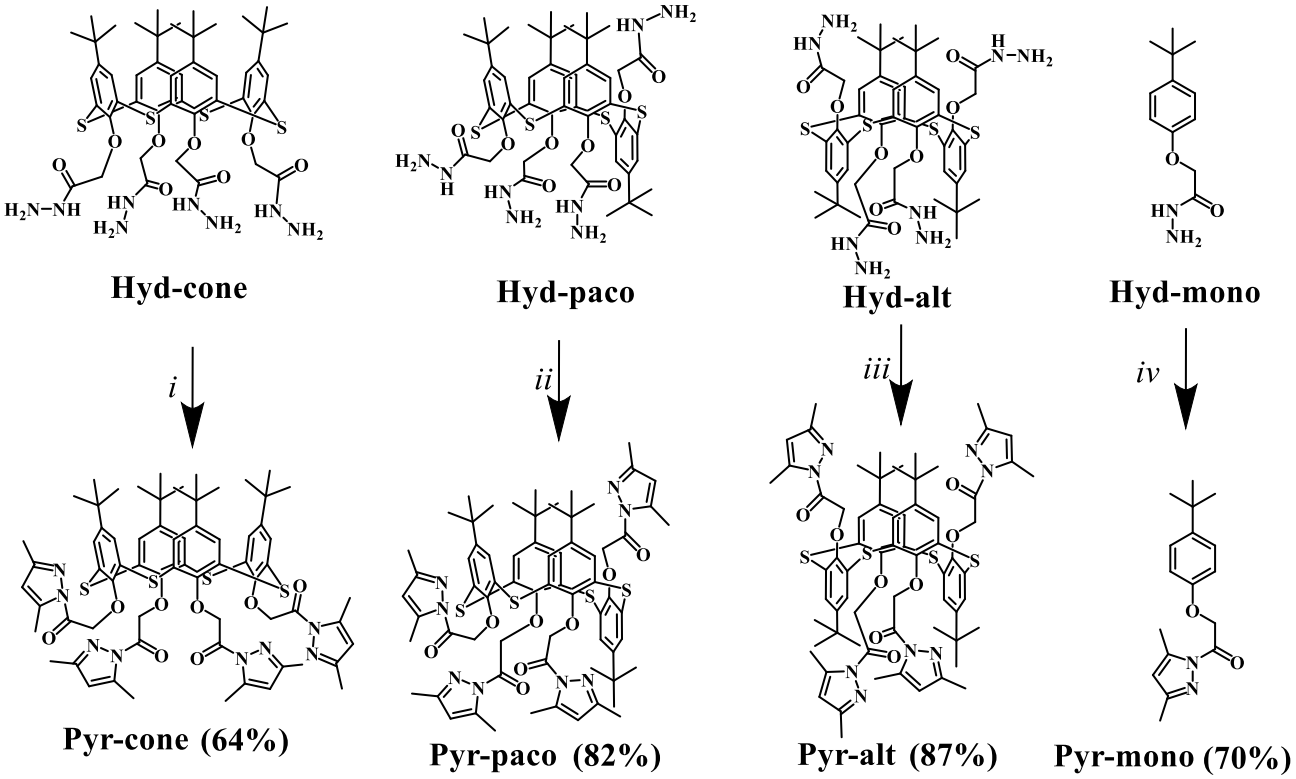

Scheme 1 Reagents and conditions: (i), acetylacetone, PTSA, $CHCl_3$, 24 h; (ii), acetylacetone, PTSA, *i*-PrOH, reflux, 12 h; (iii), acetylacetone, PTSA, *i*-PrOH, reflux, 24 h; (iv), acetylacetone, PTSA, $CHCl_3$, 2 h.

 DOI: 10.15826/chimtech.2024.11.4.18

It is noteworthy that in the transition from *1,3-alternate* to *cone* conformation, the proton signals of the oxymethylene group exhibited a pronounced upfield shift, while those of the pyrazole fragment displayed a relatively small downfield shift (Figures S2, S4). The positions of the signals can be explained by the differences in the relative position of functional groups in different stereoisomeric forms of synthesized thiacalix[4]arene. Thus, the proton signals of the oxymethylene fragments in the *1,3-alternate* (5.45 ppm) appear to be more shifted upfield due to getting into the shielding zone by aromatic fragments of the macrocycle. In contrast, the *cone* form imposes deshielding effects not only from arene fragments of the macrocyclic platform, but also from aromatic pyrazole groups, which leads to such a pronounced shift (6.32).

A similar directional change is observed for the original hydrazides (4.86 ppm – *cone*, 4.57 ppm – *1,3-alternate*), but the difference in this case is small, which can be explained by the influence of the hydrazide fragments of the initial compounds as opposed to the aromatic pyrazole fragment. In the case of displacement of proton signals of pyrazole fragments, it is obvious that in the *cone* 3,5-dimethylpyrazole fragments screen each other, and in the *1,3-alternate*, due to the distance from each other and from the arene fragments of the macrocyclic ring do not.

The ^{1}H NMR spectrum of **Pyr-paco** (Figure S3) was complicated by the symmetry-breaking of this conformational isomer in comparison with the other two forms. Therefore, the signals of the protons of the *tert*-butyl fragments were observed as three singlets at 1.07, 1.33, and 1.35 ppm, exhibiting relative intensities of 2:1:1, respectively. The protons of the methyl groups attached to the pyrazole substituents were observed in the range of 2.09–2.58 ppm.

The characteristic band in the IR spectra of **Pyr-mono**, **Pyr-cone**, **Pyr-paco** and **Pyr-alt** was the band of the average intensity of the C=N bond vibration at a value around 1590 cm^{-1} (Figures S9–S12). The obtained compounds were also characterized by MALDI MS method. The ionic peaks $[M + Na]^+$ and $[M + K]^+$ were observed for all derivatives. The mass spectra also show signals of protonated molecules (Figures S13–S16).

The spatial structure of **Pyr-alt** was fully confirmed using structural analysis by single-crystal XRD (Figure 1a). The crystals were grown from a mixture of solvents $CHCl_3$-CH_3OH. Syngony of **Pyr-alt** is triclinic, group symmetry is P-1 (Figure 1b). Crystal data, data collection, and structure refinement details are summarized in Table S1, Supplementary Materials.

3.2. The study of complexation of the 3,5-dimethylpyrazole-modificated thiacalix[4]arenes with metal cations

The resulting compounds were analyzed to determine their capacity for complexation with a range of metal cations in a chloroform-methanol (95:5) medium by UV spectroscopy method. The initial experiment involved a hundredfold excess of the following cations used in the experiment: Li, Na, Rb, Ag(I), Cu(II), Ni(II), Ca, Mg, Al, Co(III), Dy(III) and Gd(III) (Figures S17–S20). The nitrates of the corresponding metals were used as sources of cations. The interaction with Cu(II) cations was observed for all three stereoisomeric forms, resulting in a change of the character of the absorption curve across the entire significant absorption range. This led to a deviation from additivity in accordance with the Beer-Lambert law. The alterations in the absorption spectrum of **Pyr-alt** in the presence of varying cations studied are illustrated in Figure 2. It is worth noting that despite the presence of “soft” sulfur atoms, binding of Ag(I) and Ni(II) cations was not observed.

The synthesized monomer **Pyr-mono** was used to compare the binding selectivity of thiacalixarene derivatives. As the experiment with hundredfold excess of metal cations has showed, the selectivity of the monomer is appreciably lower than that of similar pyrazole derivatives of thiacalixarenes (Figure 3). It can be supposed that the pre-organized arrangement of substituents of macrocyclic derivatives **Pyr-cone**, **Pyr-paco**, and **Pyr-alt** allows obtaining selective binding of Cu(II) cations only, while the monomer compound **Pyr-mono**, according to measurements, does not possess such selectivity.

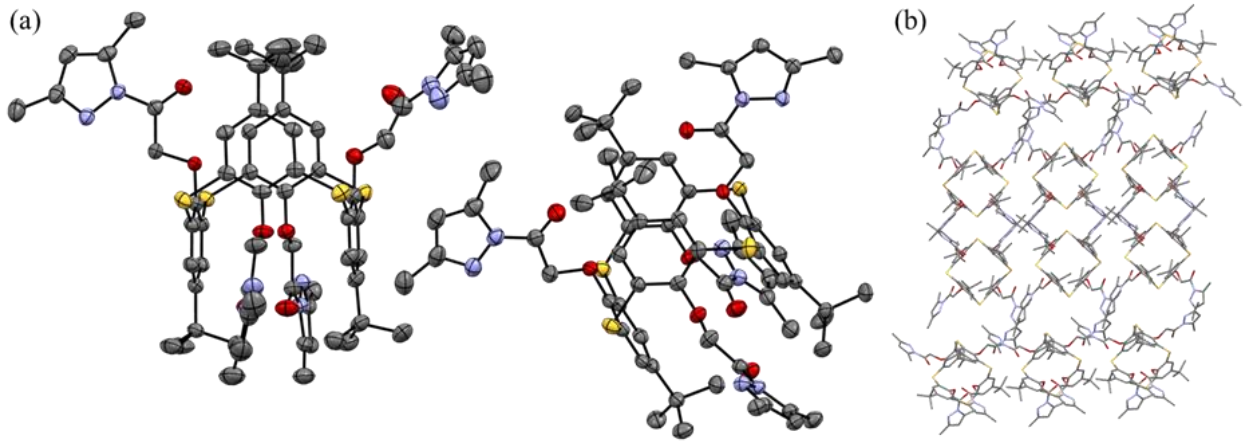

Figure 1 Molecular structure of **Pyr-alt** (a) and packaging of **Pyr-alt** in a crystal (b). Hydrogen atoms are omitted for clarity.

 DOI: 10.15826/chimtech.2024.11.4.18

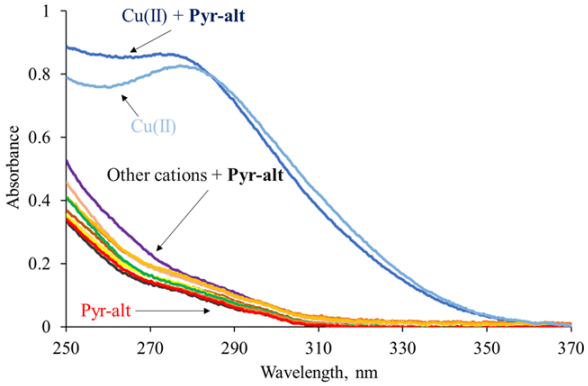

Figure 2 UV-Vis spectra of **Pyr-alt** (5 μM) with/without hundredfold excesses of nitrates (500 μM) of various s-, p-, d-, f-metals (Li(I), Na(I), Rb(I), Ag(I), Cu(II), Ni(II), Ca(II), Mg(II), Al(III), Co(III), Dy(III), Gd(III)) (CHCl3-CH3OH (95:5), 298 K).

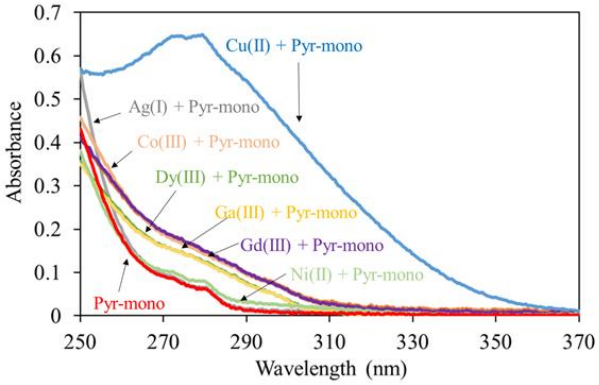

Figure 3 UV-Vis spectra of **Pyr-mono** (5 μM) with/without hundredfold excesses of nitrates (500 μM) of various p-, d-, f-metals (Ag(I), Cu(II), Ni(II), Ca(II), Mg(II), Al(III), Co(III), Dy(III), Gd(III)) ($CHCl_3$-CH_3OH (95:5), 298 K).

Next, UV-Vis titration of **Pyr-alt** with Cu(II) nitrate was carried out. The UV-Vis spectra were recorded in the range of 250–370 nm (Figure 4). A hypochromic effect was observed in the wavelength range from 250 to 270 nm when the concentration of Cu(II) cations is varied from 0.1:1 to 1:1 (Cu(II) : **Pyr-alt**). Based on the analysis of the literature data [52, 55], the electronic absorption spectra of the monomer and stereoisomers of the synthesized thiacalixarene, and the results of quantum mechanical calculations (Figure S32), it can be stated that the hypochromic effect is due to the influence of the nature of the substituent. The observed absorption corresponds to the π-π* transition in the aromatic pyrazole fragment, and binding to the metal cation leads to an increase in the energy barrier that must be overcome to realize this transition, which leads to the observed hypochromic effect.

The binding constants of Cu(II) complexes were calculated using the Bindfit program [49] based on the host-guest ratio in the resulting complex. The values of binding constants are summarized in Table 1. Also, for illustrative purposes, Table 1 includes the percentage of bound Cu(II) cations at $C_{Pyr} = C_{Cu} = 50$ mM in the case of the thiacalixarene derivatives.

The order of binding constants corresponds to literature data for pyrazole [50] and calixarene derivatives. For example, calixarenes that bind to copper(II) in the range of binding constants $5.29 \cdot 10^3$–$8.52 \cdot 10^4$ were synthesized in [51]. Comparable values were obtained and published [52]. The constants can also be higher, as in the case of [53] with an approximate value of $\log K = 7$.

As can be seen from the above data, the monomer compound **Pyr-mono** has a binding constant with Cu(II) cations three orders of magnitude higher than that of the macrocyclic derivatives obtained in the present work. This can be explained by the greater conformational mobility of the model compound compared to the rigid structures of the *p-tert*-butylthiacalixarene derivatives.

Job's plots were constructed to confirm the stoichiometry calculated from Bindfit. According to the data obtained, thiacalixarenes of all three conformations form complexes with Cu(II) cation in the ratio 1:1 (Figures S21–S23). The formation of a 1:1 complex for **Pyr-alt** (Figure 4b), despite the presence of two binding sites, can be explained by the negative allosteric effect that was described for thiacalixarenes [52, 54]. According to this view, upon binding to the Cu(II) cation, the host molecule changes its conformation in such a way that the substituents at the opposite binding site change their position relative to each other and lose the ability to bind the second guest cation.

In order to confirm the formation of the complex, a number of instrumental investigative techniques were employed. It was initially demonstrated that the Tyndall effect was not observable in the chloroform-methanol system (95:5) that was used as a solvent. This indicates that the complexes are highly soluble under these conditions. To further investigate the binding of Cu(II) cations by macrocyclic ligands, the method of ^{1}H NMR spectroscopy was applied.

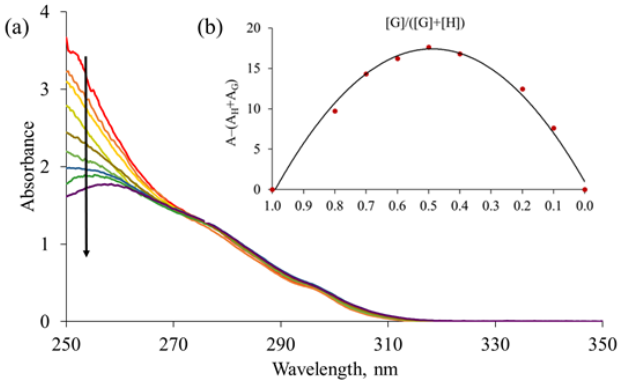

Figure 4 (a) UV-Vis titration of **Pyr-alt** (50 μM) with Cu(II) cations ($CHCl_3$-CH_3OH (95:5)) from 1:0.1 to 1:1 at 298 K. (b) Job's plot of **Pyr-alt** and Cu(II) ($CHCl_3$-CH_3OH (95:5)) at 298 K.

Table 1 Data on the complexation of the synthesized compounds with Cu(II) cations calculated from Job's and Bindfit plots.

Compound	Host-guest ratio	LogK	% of bound Cu^{2+}
Pyr-cone	1:1	4.51	46
Pyr-paco	1:1	4.63	51
Pyr-alt	1:1	4.44	44
Pyr-mono	2:1[a]	7.33	-

[a] Ratio was calculated from Bindfit source only.

 DOI: 10.15826/chimtech.2024.11.4.18

It was also taken into account that Cu(II) cations are paramagnetic, which means that their presence leads to broadening of signals as well as changes in their chemical shifts [54]. Moreover, the effect of signal broadening is proportional to the value $1/r^6$, where r is the internuclear distance between the center of the copper cation and the center of the proton under its influence. This fact allows us to estimate the proton proximity to the Cu(II) cation in the complex [52]. For this purpose, samples containing both thiacalixarenes (1 mM) with/without equimolar amounts of Cu(II) nitrate in a $CDCl_3$: CD_3OD (95:5) mixture were prepared. The concentrations of the compounds were chosen so that paramagnetic Cu(II) cations leading to broadening of the signals interfered as little as possible with their interpretation.

A preliminary experiment with **Pyr-mono** was performed to determine the binding sites. A shift of all signals is observed in ^{1}H NMR spectrum of **Pyr-mono-Cu(II)** complex (Figure 5). The proton signal of the oxymethylene group, which is close to the carbonyl pyrazole fragment but apparently far enough away from the paramagnetic Cu(II) cation, is particularly shifted from 5.40 to 4.50 ppm. The signal of the protons of the *tert*-butyl group, firstly, undergoes a shift from 1.29 ppm to 1.16 ppm, and, secondly, appeared as an extra system of three singlets at 1.20, 1.05, and 1.04 ppm. The signals of the protons of the 3,5-dimethylpyrazole fragment are highly variable. The signal of protons corresponding to one methyl group is shifted upfield; the signal of protons of another methyl fragment is shifted to the region of strong fields, while its intensity decreases due to its close proximity to the paramagnetic cation Cu(II). The signal of the pyrazole proton shifted strongly from 6.00 to 3.27 ppm due to the interaction of the pyrazole cycle with the magnetic field of the Cu(II) cation.

It can be assumed that this spectrum corresponds to the formation of two complexes, ***cis*-Pyr-mono-Cu(II)** and ***trans*-Pyr-mono-Cu(II)** (Figure 6), which also agrees with the results of the Bindfit program. The disintegration of one singlet of a *tert*-butyl group into three can be explained by the appearance of a steric barrier due to the interaction of two bulky *tert*-butyl groups of neighboring ligands. This is consistent with the "cisoidal" structure of ***cis*-Pyr-mono-Cu(II)**, and a singlet can be attributed to the "transoidal" structure of ***trans*-Pyr-mono-Cu(II)**.

In both instances, it is likely that the Cu(II) cation is bonded to the unshared electron pair of the nitrogen atoms in the pyrazole cycle and the oxygen of the carbonyl group. The existence of *cis*- and *trans*-forms of the Cu(II) complex is well documented, as proven by the example of 3,5-dimethylpyrazolidine-2,4-dione of acetic acid [55]. It can be anticipated that these structures are in dynamic equilibrium, readily transitioning between one another, given that the ratio of the relative intensities of the signals of the *tert*-butyl groups of both forms is 1:1.

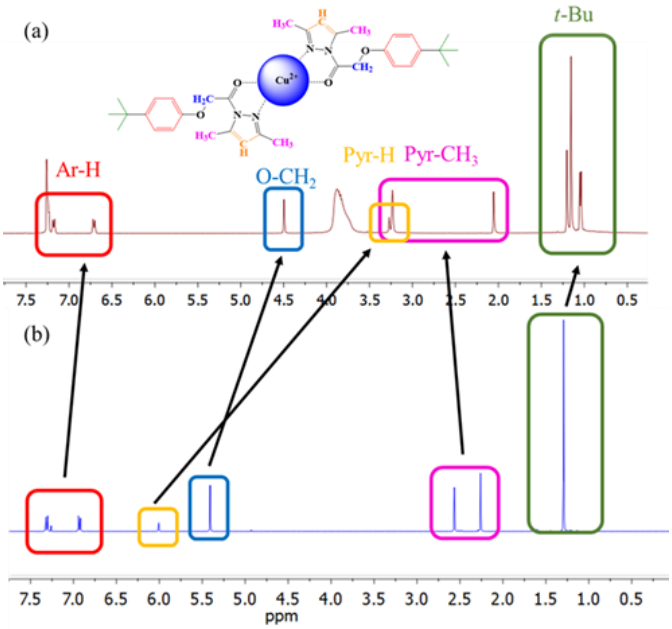

Figure 5 ^{1}H NMR spectra of (a) **Pyr-mono** (1 mM) with **Cu(II)** (1 mM) and (b) **Pyr-mono** (1 mM) ($CDCl_3$:CD_3OD (95:5), 298 K, 400 MHz).

We decided to perform DFT calculations to verify the structures of the complexes. To investigate possible structures of **Pyr-mono-Cu(II)** in solution, the DFT calculations were performed taking into account solvent effects. The methanol concentration was only about 5%, so the structures of the complexes were optimized in chloroform solution using CPCM model and one methanol molecule was explicitly put in the axial position of the complexes. The structures of two isomers with *cis* and *trans* arrangement of the ligands were optimized and are present in Figure 7. Due to repulsion of methyl groups of pyrazole fragments the coordination polyhedron of *cis* isomer is trigonal bipyramid. The values of the valence angles are: N(pyr1) – Cu – O(methanol) is 117.6°, N(pyr1) – Cu – O(carb2) is 123.8°, O(methanol) – Cu – O(carb2) is 118.1°, O(carb1) – Cu – O(methanol) is 89.4°, O(carb1) – Cu – O(carb2) is 95.0°, O(carb1) – Cu – N(pyr1) is 79.0°, N(pyr2) – Cu – O(methanol) is 91.3°, N(pyr2) – Cu – O(carb2) is 77.9°, and N(pyr2) – Cu – N(pyr1) is 107.5°. So, carbonyl oxygen of first ligand and nitrogen of pyrazole fragment of second ligand are in axial positions. Trigonal bipyramidal structure for Cu(II) complexes is not usual, but was recently observed in crystals of Cu(II) complexes with isonicotinoyl hydrazone derivative [56–58].

The structure of the coordination polyhedron of *trans* isomer is square pyramid distorted due to close arrangement of methyl and carbonyl groups of ligands. Index of the degree of trigonality (τ) for ***cis*-Pyr-mono-Cu(II)** is equal to 0.81; for ***trans*-Pyr-mono-Cu(II)** it is equal to 0.35. It means that geometry of *trans* isomer corresponds to a flatter geometry bordering on tetragonal [59]. The energy difference between these two structures is only 0.0036 a.u. = 9.5 kJ/mol.

 DOI: 10.15826/chimtech.2024.11.4.18

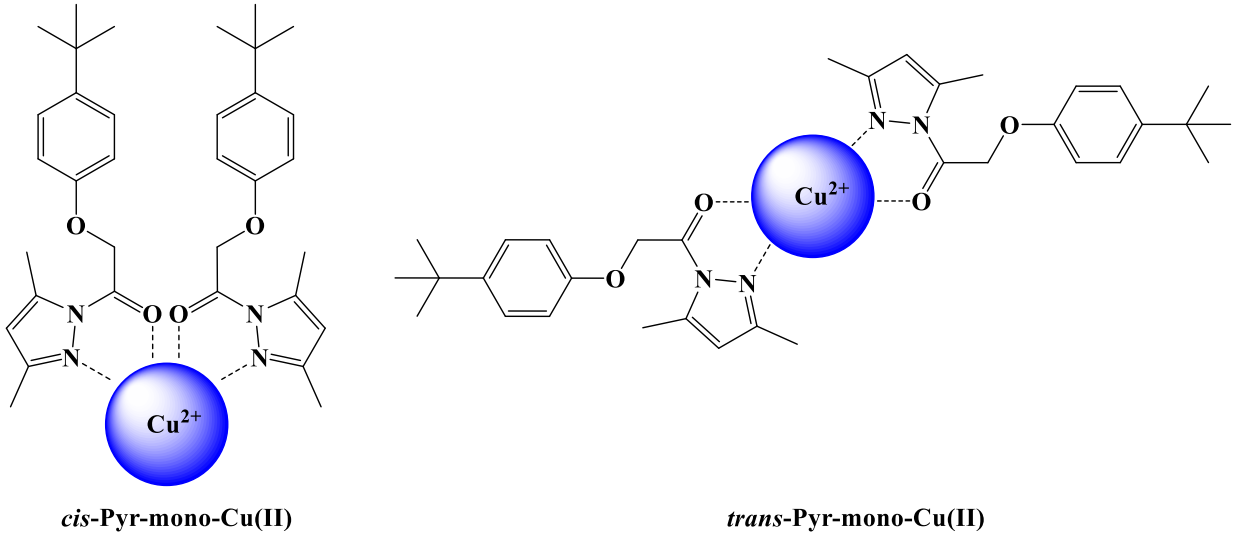

Figure 6 Possible structures of ***cis*-Pyr-mono-Cu(II)** (left) and ***trans*-Pyr-mono-Cu(II)** (right) complexes.

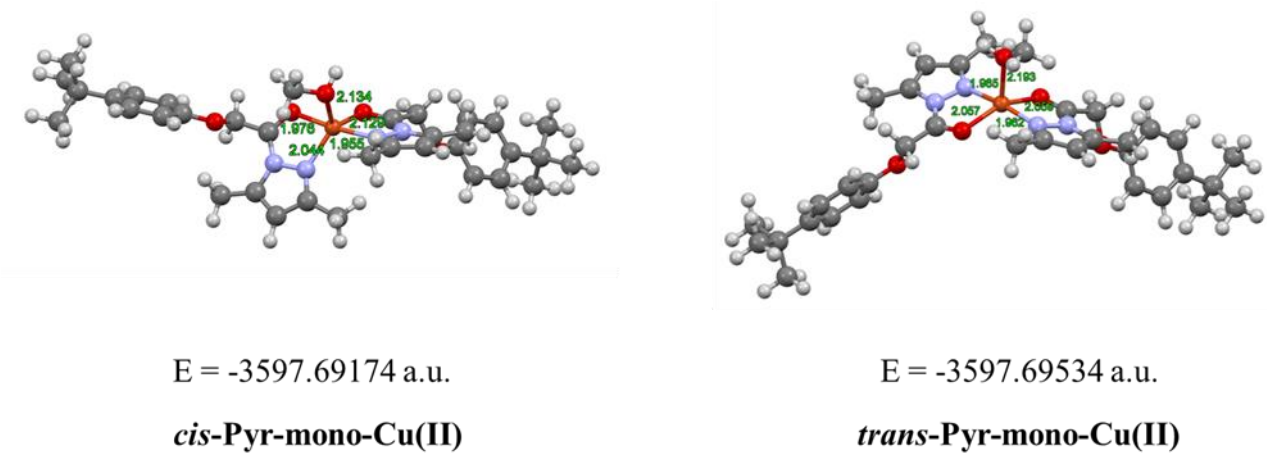

Figure 7 The structures of *cis* (left) and *trans* (right) isomers of **Pyr-mono-Cu(II)** optimized in ORCA program on the B3LYP/def2-TZVPP level, accounting for solvent effects in the C-PCM model and dispersion correction (D3DJ).

The calculated energy difference between two isomers is consistent with energy differences between *cis*- and *trans*-isomers of *bis*-amino acid Cu(II)-complexes [60–62], which both exist in solution. So we can conclude that *cis* and *trans* isomers of **Pyr-mono-Cu(II)** can also be found in solution. We also decided to simulate the UV-Vis spectrum of the **Pyr-mono-Cu(II)** complex using TD-DFT. Experimental UV-spectra were very broad, and the spectra for *cis*- and *trans*-isomers calculated by TD-DFT (Figure S32) are very close to each other. Therefore, it is not possible to determine unambiguously from UV-Vis spectra which isomer predominates in the solution.

The binding of divalent copper cations to macrocyclic ligands was also investigated using a comparable approach (Figures S29–S31). The ^{1}H NMR spectra for the free ligand (**Pyr-alt**) and the ligand bound to divalent copper (**Pyr-alt-Cu(II)**) are presented in Figure 8. The shift in the proton signals of the aromatic (from 7.47 to 7.38) and the *tert*-butyl (from 1.26 to 1.15 ppm) fragments indicates a change in the conformation of **Pyr-alt**. This indirectly supports the hypothesis of a negative allosteric effect and explains the 1:1 binding. The presence of paramagnetic Cu(II) cations results in the broadening and shifting of the proton signals associated with the 3,5-dimethylpyrazole fragment. The signals of the protons of methyl groups in close proximity to Cu(II), as well as the protons of the pyrazole cycle, are almost entirely absent. Given the relatively high lability of the complex, a relay transfer of copper cations between the ligand molecules occurs, resulting in an averaged spectrum that appears to lack free pyrazole fragments. We assume that, because, first, in the case of the NMR spectrum of **Pyr-alt-Cu(II)**, the signals of only those methyl groups of pyrazole rings that lie outside the magnetic field of copper(II) cations are observed. Second, since we observe only one signal against two in the unbound ligand, we can hypothesize that the signals are averaged due to the rapid exchange of copper cation from one ligand to another. A comparable pattern is evident in the ^{1}H NMR spectra of complexes formed by two other conformational stereoisomers as ligands (Figures S29, S30).

As NMR data show, the hydrogen signals in pyrazole substituents undergo the strongest changes, followed by the signals of oxymethylene fragments. This suggests that the copper(II) cation coordinates with one of the nitrogen

 DOI: 10.15826/chimtech.2024.11.4.18

atoms of the pyrazole fragment and the oxygen of the carbonyl group. In addition, we assume that only two pyrazole cycles in all three stereoisomeric forms participate in copper(II) binding. We conclude that the other two pyrazole rings are not involved from the following: 1) for all forms, 1:1 stoichiometry is observed, even for the *1,3-alternate*, and 2) the pyrazole fragments appear differently in the NMR spectra. Relatively small shifts of proton signals of the aromatic ring and *tert*-butyl substituents at the upper rim are also observed. The latter fact can be explained by a general change in the conformation of the macrocycle.

Thus, in the presented work, we developed a methodology for the synthesis of the *p-tert*-butylthiacalix[4]arene 3,5-dimethylpyrazole derivatives **Pyr-cone**, **Pyr-paco,** and **Pyr-alt**, as well as the monomeric compound **Pyr-mono** from the corresponding hydrazides. The obtained compounds were characterized by a set of physical methods (^{1}H and ^{13}C{^{1}H} NMR, IR, MALDI mass spectrometry, elemental analysis). **Pyr-cone**, **Pyr-paco** and **Pyr-alt** were shown to bind selectively to Cu(II) cations; the binding constants and stoichiometry of such complexes were calculated. On the example of **Pyr-mono-Cu(II)** complex calculated by DFT method and investigated by ^{1}H NMR spectroscopy, the possibility of existence of cisoidal and transoidal structures of this complex was shown.

4. Limitations

The obtained 3,5-dimethylpyrazole derivatives of *p-tert*-butylthiacalix[4]arenes, selectively binding Cu(II) cations, are well soluble in organochlorine compounds, DMSO and DMF, but their solubility in polar proton solvents is extremely limited, which determines the zone of action of such compounds for the detection of Cu(II) cations only under *in vitro* conditions.

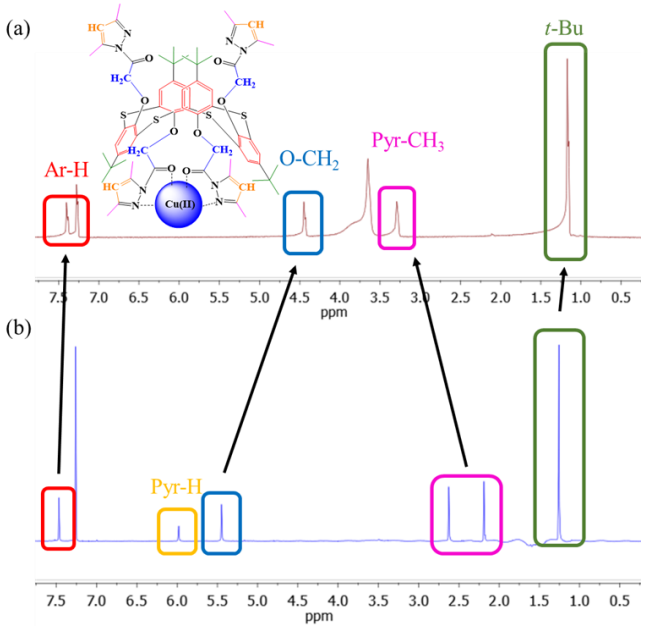

Figure 8 ^{1}H NMR spectra of (a) complex of **Pyr-alt** (1 mM) with **Cu(II)** (1 mM) and (b) **Pyr-alt** (1 mM) ($CDCl_3$: CD_3OD (95:5), 298 K, 400 MHz).

5. Conclusions

In this study, we synthesized thiacalixarenes modified with 3,5-dimethylpyrazole moieties in three stereoisomeric forms (*cone*, *partial cone*, and *1,3-alternate*) for the first time in high yields. The obtained compounds were characterized by a set of instrumental methods, including single-crystal XRD, NMR, UV-Vis, IR spectroscopy, MALDI MS, and elemental analysis. The formation of complexes with Cu(II) cations in a chloroform-methanol solution was investigated. Cu(II) selective binding with **Pyr-cone**, **Pyr-paco** and **Pyr-alt** (log$K$ = 4.44–4.63, 1:1 stoichiometry), and **Pyr-mono** (log$K$ = 7.33, 2:1 stoichiometry) was shown by UV-Vis spectroscopy. It was demonstrated that the selectivity of complex formation of the model compound **Pyr-mono** was lower and the binding constant with Cu(II) was higher in comparison to its macrocyclic analogues. It can be explained by the lower steric hindrance of the model compound and the absence of stereoisomeric rigidity inherent in thiacalixarenes. The energies of potential structures of the **Pyr-mono-Cu(II)** complex (***cis*-Pyr-mono-Cu(II)** and ***trans*-Pyr-mono-Cu(II)**) were calculated using DFT. The energy difference between these two structures is only 0.0036 a.u. = 9.5 kJ/mol (the *trans*-isomer is slightly more stable). It was also postulated that the Cu(II) cation binds to thiacalixarenes at the pyrazole cycle and the carbonyl oxygen atom, with the sulfur atom remaining uninvolved in the binding. The results obtained may be useful for the development of thiacalix[4]arene derivatives containing pyrazole moieties for the selective detection of Cu(II) cations, which may be particularly useful for the diagnosis of diseases related to copper metabolism (Wilson's and Menkes diseases). Also, the data from this work are useful for those concerned with the mechanism of formation of complexes with heterocyclic ligands.

• Supplementary materials

Figures S1–S4: ^{1}H NMR spectra of **Pyr-mono**, **Pyr-cone**, **Pyr-paco** and **Pyr-alt**; **Figures S5–S8**. ^{13}C{^{1}H} NMR spectra of **Pyr-mono**, **Pyr-cone**, **Pyr-paco** and **Pyr-alt**; **Figures S9–S12**. FT-IR spectra of **Pyr-mono**, **Pyr-cone**, **Pyr-paco** and **Pyr-alt**; **Figures S13–S16**. HRMS spectra of **Pyr-mono**, **Pyr-cone**, **Pyr-paco** and **Pyr-alt**; **Figures S17–S20:** UV-Vis spectra of **Pyr-mono**, **Pyr-cone**, **Pyr-paco** and **Pyr-alt** without/with 100-fold excess of metal cations; **Figures S21–S23:** Job's plots for the determination of the stoichiometry in the complexes of **Pyr-cone-Cu(II)**, **Pyr-paco-Cu(II)**, **Pyr-alt-Cu(II)**; **Figures S24–S27**: UV-Vis spectra of **Pyr-mono**, **Pyr-cone**, **Pyr-paco**, and **Pyr-alt** with Cu(II) cations; **Figures S28–S31:** ^{1}H NMR spectra of **Pyr-mono**, **Pyr-cone**, **Pyr-paco** and **Pyr-alt** upon addition of Cu(II). **Figure S32**: Simulated UV-Vis spectra of the complex **Pyr-mono-Cu(II)**. **Table S1.** Crystal data and structure refinement for **Pyr-alt.**

 DOI: 10.15826/chimtech.2024.11.4.18

• Funding

The work was financially supported by the Priority-2030 Strategic Academic Leadership Program, Kazan (Volga Region) Federal University.

• Acknowledgments

MALDI MS data were obtained in the CSF-SAC FRC KSC RAS by support of the State Assignment of the Federal Research Center “Kazan Scientific Center”, Russian Academy of Sciences.

• Author contributions

Conceptualization: I.S.
Data curation: E.R., O.B., D.I., M.B.
Formal Analysis: V.K. M.B., O.B., D.I.
Funding acquisition: I.S.
Investigation: V.K., E.R., M.B., K.S, O.B., D.I.
Methodology: V.K., I.S.
Project administration: I.S.
Software: M.B.
Supervision: K.S., I.S.
Validation: E.R., K.S.
Visualization: V.K.
Writing – original draft: V.K.
Writing – review & editing: I.S.

• Conflict of interest

The authors declare no conflict of interest.

• Additional information

Author IDs:
Valeriy Kalinin, Scopus ID 57212313589;
Mikhail Bukharov, Scopus ID 54895268200;
Daut Islamov, Scopus ID 15128759500;
Ivan Stoikov, Scopus ID 6602887534.

Websites:
Kazan Federal University, https://eng.kpfu.ru/;
FRC Kazan Scientific Center, https://knc.ru/en/.

References

1. Crisponi G, Nurchi VM, Fanni D, Gerosa C, Nemolato S, Faa G. Copper-related diseases: from chemistry to molecular pathology. Coord Chem Rev. 2010;254(7–8):876–889. doi:10.1016/j.ccr.2009.12.018
2. Tümer Z, Møller LB. Menkes disease. Eur J Hum Genet. 2010;18(5):511–518. doi:10.1038/ejhg.2009.187
3. Purchase R. The link between copper and Wilson's Disease. Sci Prog. 2013;96(3):213–223. doi:10.3184/003685013X13712193905878
4. Ahuja A, Dev K, Tanwar RS, Selwal KK, Tyagi PK. Copper mediated neurological disorder: visions into amyotrophic lateral sclerosis, alzheimer and menkes disease. J Trace Elements Med Biol. 2015;29(1):11–23. doi:10.1016/j.jtemb.2014.05.003
5. Więcek S, Paprocka J. Disorders of copper Metabolism in Children—A problem too rarely Recognized. Metabolites. 2024;14(1):38. doi:10.3390/metabo14010038
6. Hung YH, Bush AI, Cherny RA. Copper in the brain and Alzheimer’s disease. JBIC J Biol Inorg Chem. 2010;15(1):61–76. doi:10.1007/s00775-009-0600-y
7. Bisaglia M, Bubacco L. Copper ions and Parkinson’s Disease: why Is homeostasis So Relevant?. Biomolecules. 2020;10(2):195. doi:10.3390/biom10020195
8. Koutsouraki E, Michmizos D, Patsi O, Tzartos J, Spilioti M, Arnaoutoglou M, Tsolaki M. A probable role of copper in the comorbidity in Wilson’s and Creutzfeldt-Jakob’s Diseases: a case report. Virol J. 2020;17(1). doi:10.1186/s12985-020-01309-x
9. Duncan C, White AR. Copper complexes as therapeutic agents. Metallomics. 2011;4(2):127–138. doi:10.1039/c2mt00174h
10. Gromadzka G, Grycan M, Przybyłkowski AM. Monitoring of copper in wilson Disease. Diagnostics. 2023;13(11):1830. doi:10.3390/diagnostics13111830
11. Liu H, Li FX, Pi Y, Wang DJ, Hu YJ, Zheng J. Fluorescence quenching study of 2,6-bis(5-(4-methylphenyl)-1- H -pyrazol-3-yl)pyridine with metal ions. Spectrochim Acta Part A Mol Biomol Spectrosc. 2015;145:588–593. doi:10.1016/j.saa.2015.03.049
12. Zhao J, Zhang L, Huang Q, Ma D, Ren T. A near-infrared AIEE fluorescent chemosensor for Cu^{2+} through an IPT process. Inorg Chim Acta. 2023;555:121579. doi:10.1016/j.ica.2023.121579
13. Mithra U, Sarveswari, S. A review on pyrazole moieties as organic chemosensors in the detection of cations and anions. Inorg Chim Acta. 2024;569:122118. doi:10.1016/j.ica.2024.122118
14. Hu Q, Song YF, Wu WN, Zhao XL, Wang Y, Fan YC. A coumarin-pyrazole-based probe for the fluorescence detection of phosgene with high selectivity and sensitivity. Anal Methods. 2023;15(22):2761–2765. doi:10.1039/D3AY00516J
15. Turones LC, Martins AN, Moreira LKS, Fajemiroye JO, Costa EA. Development of pyrazole derivatives in the management of inflammation. Fundam Clin Pharmacol. 2021;35(2):217–234. doi:10.1111/fcp.12629
16. Ravindar L, Hasbullah SA, Rakesh KP, Hassan NI. Pyrazole and pyrazoline derivatives as antimalarial agents: A key review. Eur J Pharm Sci. 2023;183:106365. doi:10.1016/j.ejps.2022.106365
17. Lorthiois E, Gerspacher M, Beyer KS, Vaupel A, Leblanc C, Stringer R, Weiss A, Wilcken R, Guthy DA, Lingel A, Bomio-Confaglia C, Machauer R, Rigollier P, Ottl J, Arz D, Bernet P, Desjonqueres G, Dussauge S, Kazic-Legueux M, Lozac’h MA, Mura C, Sorge M, Todorov M, Warin N, Zink F, Voshol H, Zecri FJ, Sedrani RC, Ostermann N, Brachmann SM, Cotesta S. JDQ443, a structurally Novel, Pyrazole-Based, covalent Inhibitor of KRASG12C for the treatment of solid Tumors. J Med Chem. 2022;65(24):16173–16203. doi:10.1021/acs.jmedchem.2c01438
18. Shchegolkov EV, Perminova AN, Malkova NA, Kushch SO, Burgart YV, Triandafilova GA, Solodnikov SY, Krasnykh OP, Saloutin VI. Modifications of 4-Amino-substituted 5-Phenyl-3-(trifluoromethyl)pyrazoles for the development of new Analgesics. ChemistrySelect. 2023;8(47). doi:10.1002/slct.202303265
19. dos Santos GC, Martins LM, Bregadiolli BA, Moreno VF, da Silva-Filho LC, da Silva BHST. Heterocyclic compounds as antiviral drugs: Synthesis, structure–activity relationship and traditional applications. J Heterocycl Chem. 2021;58(12):2226–2260. doi:10.1002/jhet.4349
20. Hemdan BA, Radwan EK, Rashdan HRM. Design and solvent free synthesis of novel phenazone based molecule for water disinfection and rapid removal of the anionic direct fast blue

B2RL dye. J Water Process Eng. 2023;54:103861. doi:10.1016/j.jwpe.2023.103861
21. Althomali RH, Alamry KA, Hussein MA, Guedes RM. An investigation on the adsorption and removal performance of a carboxymethylcellulose-based 4-aminophenazone@MWCNT nanocomposite against crystal violet and brilliant green dyes. RSC Adv. 2023;13(7):4303–4313. doi:10.1039/D2RA07321H
22. Silva F, Costa G, Veiga F, Cardoso C, Paiva-Santos AC. Parenteral Ready-to-use Fixed-dose Combinations including NSAIDs with paracetamol or metamizole for multimodal Analgesia—approved Products and Challenges. Pharmaceuticals. 2023;16(8):1084. doi:10.3390/ph16081084
23. Yushkova EA, Stoikov II, Zhukov AY, Puplampu JB, Rizvanov IK, Antipin IS, Konovalov A. Heteroditopic p-tert-butyl thiacalix[4]arenes for creating supramolecular self-assembles by cascade or commutative mechanisms. RSC Adv. 2012;2(9):3906. doi:10.1039/C2RA01255C
24. Padnya PL, Andreyko EA, Gorbatova PA, Parfenov VV, Rizvanov IK, Stoikov II. Towards macrocyclic ionic liquids: novel ammonium salts based on tetrasubstituted p-tert-butylthiacalix[4]arenes. RSC Adv. 2017;7(3):1671–1686. doi:10.1039/C6RA24734B
25. Stoikov II, Yushkova EA, Bukharaev AA, Biziaev DA, Selivanovskaya SY, Chursina MA, Antipin IS, Konovalov AI, Zharov I. Self-assembly of p-tert-butyl thiacalix[4]arenes and metal cations into nanoscale three-dimensional particles. J Phys Org Chem. 2012;25(12):1177–1185. doi:10.1002/poc.2981
26. Yakimova L, Kunafina A, Nugmanova A, Padnya P, Voloshina A, Petrov K, Stoikov I. Structure–activity Relationship of the Thiacalix[4]arenes family with sulfobetaine Fragments: Self-assembly and cytotoxic Effect against cancer Cell Lines. Molecules. 2022;27(4):1364. doi:10.3390/molecules27041364
27. Padnya PL, Terenteva OS, Akhmedov AA, Iksanova AG, Shtyrlin NV, Nikitina EV, Krylova ES, Shtyrlin YG, Stoikov II. Thiacalixarene based quaternary ammonium salts as promising antibacterial agents. Bioorg Med Chem. 2021;29:115905. doi:10.1016/j.bmc.2020.115905
28. Shiabiev I, Pysin D, Akhmedov A, Babaeva O, Babaev V, Lyubina A, Voloshina A, Petrov K, Padnya P, Stoikov I. Towards antibacterial Agents: synthesis and biological Activity of multivalent Amide derivatives of Thiacalix[4]arene with hydroxyl and amine Groups. Pharmaceutics. 2023;15(12):2731. doi:10.3390/pharmaceutics15122731
29. Nazarova A, Shiabiev I, Shibaeva K, Mostovaya O, Mukhametzyanov T, Khannanov A, Evtugyn V, Zelenikhin P, Shi X, Shen M, Padnya P, Stoikov I. Thiacalixarene carboxylic Acid derivatives as inhibitors of lysozyme Fibrillation. Int J Mol Sci. 2024;25(9):4721. doi:10.3390/ijms25094721
30. Alekseeva EA, Krasnoshchekaya SP, Gren' AI. Synthesis of p-tert-Butylcalix[4]arene Derivatives Containing Acylpyrazole Fragments. Russ J Gen Chem. 2002;72(1):157–159. doi:10.1023/A:1015386505286
31. Muravev AA, Voloshina AD, Sapunova AS, Gabdrakhmanova FB, Lenina OA, Petrov KA, Shityakov S, Skorb EV, Solovieva SE, Antipin IS. Calix[4]arene–pyrazole conjugates as potential cancer therapeutics. Bioorg Chem. 2023;139:106742. doi:10.1016/j.bioorg.2023.106742
32. Chen YJ, Chen MY, Lee KT, Shen LC, Hung HC, Niu HC, Chung WS. 1,3-alternate Calix[4]arene functionalized With pyrazole and triazole Ligands as a highly Selective fluorescent Sensor for Hg^{2+} and Ag^{+} Ions. Front Chem. 2020;8. doi:doi.org/10.3389/fchem.2020.593261
33. Abdou A, Omran OA, Al-Fahemi JH, Jassas RS, Al-Rooqi MM, Hussein EM, Moussa Z, Ahmed SA. Lower rim thiacalixarenes derivatives incorporating multiple coordinating carbonyl groups: Synthesis, characterization, ion-responsive ability and DFT computational analysis. J Mol Struct. 2023;1293:136264. doi:10.1016/j.molstruc.2023.136264
34. KILIÇ HURYEAKDA, GRAF ERNEST, HOSSEİNİ MRWAS, KYRİTSAKAS NATHALE. New 2-D silver(I) coordination network constructed from thiomethyl group-substituted p-tert-butylthiacalix[4]arene. Turk J Chem. 2022;46(5):1541–1547. doi:10.55730/1300-0527.3459
35. Fang Y, Xie WX, Han K, Zhou K, Kang L, Shi J, Chen BK, Bi YF. Diphosphine modified copper(I)-thiacalixarene supramolecular structure for effective photocurrent response and photodegradation of methylene blue. Polyhedron. 2022;222:115934. doi:10.1016/j.poly.2022.115934
36. Zhou Z, Xu L, Zhao G, Zhou K, Chen B, Bi Y. An ultra-stable CuI12 cluster built from a CuI6 precursor sandwiched by two CuI3-thiacalixarene units for efficient photothermal conversion. Inorg Chem Front. 2023;10(11):3230–3236. doi:10.1039/D3QI00479A
37. Wang Z, Su HF, Gong YW, Qu QP, Bi YF, Tung CH, Sun D, Zheng LS. A hierarchically assembled 88-nuclei silver-thiacalix[4]arene nanocluster. Nat Commun. 2020;11(1). doi:10.1038/s41467-019-13682-5
38. Takagiri Y, Ikuta T, Maehashi K. Selective detection of Cu2+ ions by immobilizing Thiacalix[4]arene on graphene Field-effect Transistors. ACS Omega. 2020;5(1):877–881. doi:10.1021/acsomega.9b03821
39. Evtugyn GA, Stoikov II, Beljyakova SV, Shamagsumova RV, Stoikova EE, Zhukov AY, Antipin IS, Budnikov HC. Ag selective electrode based on glassy carbon electrode covered with polyaniline and thiacalix[4]arene as neutral carrier. Talanta. 2007;71(4):1720–1727. doi:10.1016/j.talanta.2006.08.004
40. Mostovaya O, Padnya P, Shiabiev I, Mukhametzyanov T, Stoikov I. PAMAM-calix-dendrimers: synthesis and thiacalixarene Conformation effect on DNA Binding. Int J Mol Sci. 2021;22(21):11901. doi:10.3390/ijms222111901
41. Subashini G, Saravanan A, Shyamsivappan S, Arasakumar T, Mahalingam V, Shankar R, Mohan PS. A versatile “on-off-on” quinoline pyrazoline hybrid for sequential detection of Cu2+ and S– ions towards bio imaging and tannery effluent monitoring. Inorg Chim Acta. 2018;483:173–179. doi:10.1016/j.ica.2018.08.012
42. Nguyen VA, Vu TNA, Polyanskaya N, Utenyshev A, Shilov G, Vasil'eva M, Anh Tien N, Kovalchukova O. Structure and properties of some S-containing azo-derivatives of 5-pyrazolone and their Cu(II), Co(II), and Ni(II) metal complexes. Inorg Chem Commun. 2023;158:111648. doi:10.1016/j.inoche.2023.111648
43. Radnović ND, Štetin N, Radanović MM, Borišev I, Rodić MV, Jaćimović K, Barta Holló B. Two isomers of a novel Ag(I) complex with Pyrazole-type Ligand—Synthesis, Structural, Thermal, and antioxidative Characterization. Inorg. 2023;12(1):4. doi:10.3390/inorganics12010004
44. Stoikov II, Yushkova EA, Zharov I, Antipin IS, Konovalov AI. Supramolecular self-assemblies of stereoisomers of p-tert-butyl thiacalix[4]arenes functionalized with hydrazide groups at the lower rim with some metal cations. Tetrahedron. 2009;65(34):7109–7114. doi:10.1016/j.tet.2009.06.045
45. Hoover JM, DiPasquale A, Mayer JM, Michael FE. Platinum-catalyzed Intramolecular Hydrohydrazination: evidence for alkene Insertion into a Pt–N Bond. J Am Chem Soc. 2010;132(14):5043–5053. doi:10.1021/ja906563z
46. Hashem HE, Ahmad S, Kumer A, Bakri YE. In silico and in vitro prediction of new synthesized N-heterocyclic compounds as anti-SARS-CoV-2. Sci Rep. 2024;14(1). doi:10.1038/s41598-024-51443-7
47. Mohamed MA, Ali A, Ali A, Afzal O, Ahsan MF, Alamri MA, Alossaimi MA, Altamimi ASA, Salahuddin, Ahsan MJ. Targeting EGFR by newer 1-(3,5-Bis((E)-4 hydroxy-3-methoxystyryl)-1H-pyrazol-1-yl)-2-((substituted phenyl)amino)ethan-1-one analogues for the treatment of Cancer: Synthesis, In-vitro and In-silico Studies. J Mol Struct. 2024;1315:138826. doi:10.1016/j.molstruc.2024.138826
48. Staab H.;Bauer H.;Schneider K. Azolides in organic Synthesis and Biochemistry. 1st ed. Wiley-VCH GmbH & Co. KGaA: Weinheim, Germany. 27–79. doi:10.1002/3527600833

 DOI: 10.15826/chimtech.2024.11.4.18

49. Bindfit. Available online: http://supramolecular.org (accessed on 20 September 2024)
50. Gu YQ, Shen WY, Zhou Y, Chen SF, Mi Y, Long BF, Young DJ, Hu FL. A pyrazolopyrimidine based fluorescent probe for the detection of Cu^{2+} and Ni^{2+} and its application in living cells. Spectrochim Acta Part A Mol Biomol Spectrosc. 2019;209:141–149. doi:10.1016/j.saa.2018.10.030
51. Costa AI, Barata PD, Fialho CB, Prata JV. Highly sensitive and selective Fluorescent probes for Cu(II) detection Based on Calix[4]arene-oxacyclophane Architectures. Molecules. 2020;25(10):2456. doi:10.3390/molecules25102456
52. Padnya P, Shibaeva K, Arsenyev M, Baryshnikova S, Terenteva O, Shiabiev I, Khannanov A, Boldyrev A, Gerasimov A, Grishaev D, Shtyrlin Y, Stoikov I. Catechol-containing Schiff bases on Thiacalixarene: Synthesis, copper (II) Recognition, and formation of Organic-inorganic Copper-based Materials. Molecules. 2021;26(8):2334. doi:10.3390/molecules26082334
53. Qazi MA, Ocak, Ocak M, Memon S. An excellent copper selective chemosensor based on calix[4]arene framework. Anal Chim Acta. 2013;761:157–168. doi:10.1016/j.aca.2012.11.026
54. Pandey R, Kumar A, Xu Q, Pandey DS. Zinc(ii), Cu(II) and cadmium(ii) complexes as fluorescent chemosensors for cations. Dalton Trans. 2019;49(3):542–568. doi:10.1039/C9DT03017D
55. Ishihara K, Nishimura K, Yamakawa K. Enantio- and Site-selective α-fluorination of N-acyl 3,5-dimethylpyrazoles Catalyzed by chiral π–CuII Complexes. Angew Chem Int Ed. 2020;59(40):17641–17647. doi:10.1002/anie.202007403
56. Ahmed MA, Zhernakov MA, Gilyazetdinov EM, Bukharov MS, Islamov DR, Usachev KS, Klimovitskii AE, Serov NY, Burilov VA, Shtyrlin VG. Complexes of NiII, CoII, ZnII, and CuII with promising Anti-tuberculosis Drug: Solid-state Structures and DFT Calculations. Inorg. 2023;11(4):167. doi:10.3390/inorganics11040167
57. Serov NY, Shtyrlin VG, Bukharov MS, Ermolaev AV, Gilyazetdinov EM, Urazaeva KV, Rodionov AA. Complex structures, formation thermodynamics and substitution reaction kinetics in the Cu(II) – glycylglycyl-l-tyrosine – l/d-histidine systems. Polyhedron. 2022;228:116176. doi:10.1016/j.poly.2022.116176
58. Shtyrlin VG, Serov NY, Bukharov MS, Gilyazetdinov EM, Zhernakov MA, Ahmed MA, Garifzyanov AR, Mirzayanov II, Ermolaev AV, Aksenin NS, Urazaeva KV, Zakharov AV. Stereoselective effects, formation thermodynamics, substitution reaction kinetics, and structures of transition metal complexes with bioligands and aromatic N-donors. Russ Chem Bull. 2023;72(7):1485–1498. doi:10.1007/s11172-023-3926-7
59. Addison AW, Rao TN, Reedijk J, van Rijn J, Verschoor GC. Synthesis, structure, and spectroscopic properties of copper(II) compounds containing nitrogen–sulphur donor ligands;the crystal and molecular structure of aqua[1,7-bis(N-methylbenzimidazol-2′-yl)-2,6-dithiaheptane]copper(II) perchlorate. J Chem Soc Dalton Trans. 2004;7:1349–1356. doi:10.1039/DT9840001349
60. Shtyrlin VG, Zyavkina YI, Ilakin VS, Garipov RR, Zakharov AV. Structure, stability, and ligand exchange of Cu(II) complexes with oxidized glutathione. J Inorg Biochem. 2005;99(6):1335–1346. doi:10.1016/j.jinorgbio.2005.03.008
61. Powell DH, Helm L, Merbach AE. 17O nuclear magnetic resonance in aqueous solutions of Cu^{2+}: the combined effect of Jahn–Teller inversion and solvent exchange on relaxation rates. J Chem Phys. 1991;95(12):9258–9265. doi:10.1063/1.461206
62. Bukharov MS, Shtyrlin VG, Mukhtarov AS, Mamin GV, Stapf S, Mattea C, Krutikov AA, Il'in AN, Serov NY. Study of structural and dynamic characteristics of Cu(II) amino acid complexes in solutions by combined EPR and NMR relaxation methods. Phys Chem Chem Phys. 2014;16(20):9411. doi:10.1039/c4cp00255e
63. Neese F. The ORCA program system. WIREs Comput Mol Sci. 2012;2(1):73–78. doi:10.1002/wcms.81
64. Kohn W, Becke AD, Parr RG. Density functional Theory of electronic Structure. J Phys Chem. 1996;100(31):12974–12980. doi:10.1021/jp9606691
65. Becke AD. Density-functional thermochemistry. III. the role of exact exchange. J Chem Phys. 1993;98(7):5648–5652. doi:10.1063/1.464913
66. Lee C, Yang W, Parr RG. Development of the Colle-salvetti correlation-energy formula into a functional of the electron density. Phys Rev B. 2002;37(2):785–789. doi:10.1103/PhysRevB.37.785
67. Schäfer A, Huber C, Ahlrichs R. Fully optimized contracted gaussian basis sets of triple zeta valence quality for atoms li to Kr. J Chem Phys. 1994;100(8):5829–5835. doi:10.1063/1.467146
68. Weigend F, Ahlrichs R. Balanced basis sets of split valence, triple zeta valence and quadruple zeta valence quality for H to Rn: design and assessment of accuracy. Phys Chem Chem Phys. 2005;7(18):3297. doi:10.1039/B508541A
69. Weigend F, Häser M, Patzelt H, Ahlrichs R. RI-MP2: optimized auxiliary basis sets and demonstration of efficiency. Chem Phys Lett. 1998;294(1–3):143–152. doi:10.1016/S0009-2614(98)00862-8
70. Cossi M, Rega N, Scalmani G, Barone V. Energies, structures, and electronic properties of molecules in solution with the C-PCM solvation model. J Comput Chem. 2003;24(6):669–681. doi:10.1002/jcc.10189
71. Grimme S, Antony J, Ehrlich S, Krieg H. A consistent and accurateab initioparametrization of density functional dispersion correction (DFT-D) for the 94 elements H-Pu. J Chem Phys. 2010;132(15):1. doi:10.1063/1.3382344
72. Grimme S, Ehrlich S, Goerigk L. Effect of the damping function in dispersion corrected density functional theory. J Comput Chem. 2011;32(7):1456–1465. doi:10.1002/jcc.21759
73. Sheldrick GM. SHELXT– integrated space-group and crystal-structure determination. Acta Crystallogr Sect Adv. 2015;71(1):3–8. doi:10.1107/S2053273314026370
74. Sheldrick GM. A short history of SHELX. Acta Crystallogr Sect Crystallogr. 2008;64(1):112–122. doi:10.1107/S0108767307043930
75. Macrae CF, Edgington PR, McCabe P, Pidcock E, Shields GP, Taylor R, Towler M, van de Streek J. Mercury: visualization and analysis of crystal structures. J Appl Crystallogr. 2006;39(3):453–457. doi:10.1107/S002188980600731X
76. Wang Y, Lu X, Shi J, Xu J, Wang F, Yang X, Yu G, Liu Z, Li C, Dai A, Zhao Y, Wu J. Synthesis and larvicidal activity of 1,3,4-oxadiazole derivatives containing a 3-chloropyridin-2-yl-1H-pyrazole scaffold. Monatshefte für Chem. Chem Mon. 2018;149(3):611–623. doi:10.1007/s00706-017-2060-3

 DOI: 10.15826/chimtech.2024.11.4.18